Geoscience Frontiers 8 (2017) 1311–1321

HOSTED BY

Contents lists available at ScienceDirect

China University of Geosciences (Beijing)

Geoscience Frontiers

journal homepage: www.elsevier.com/locate/gsf

Research Paper

The production of iron oxide during peridotite serpentinization: Influence of pyroxene

Ruifang Huang [a,b,*], Chiou-Ting Lin [a], Weidong Sun [a], Xing Ding [c], Wenhuan Zhan [b], Jihao Zhu [d]

[a] Key Laboratory of Mineralogy and Metallogeny, Guangzhou Institute of Geochemistry, Chinese Academy of Sciences, Guangzhou 510640, PR China
[b] Key Laboratory of Marginal Sea Geology, South China Sea Institute of Oceanology, Chinese Academy of Sciences, Guangzhou 510301, PR China
[c] State Key Laboratory of Isotope Geochemistry, Guangzhou Institute of Geochemistry, Chinese Academy of Sciences, Guangzhou 510640, PR China
[d] The Second Institute of Oceanography, SOA, Hangzhou 310012, PR China

ARTICLE INFO

Article history:
Received 3 August 2016
Received in revised form
4 December 2016
Accepted 9 January 2017
Available online 25 January 2017
Handling Editor: Y. Eyuboglu

Keywords:
Serpentinization
Iron oxide
Peridotite
Orthopyroxene
Silica
Aluminum

ABSTRACT

Serpentinization produces molecular hydrogen (H_2) that can support communities of microorganisms in hydrothermal fields; H_2 results from the oxidation of ferrous iron in olivine and pyroxene into ferric iron, and consequently iron oxide (magnetite or hematite) forms. However, the mechanisms that control H_2 and iron oxide formation are poorly constrained. In this study, we performed serpentinization experiments at 311 °C and 3.0 kbar on olivine (with <5% pyroxene), orthopyroxene, and peridotite. The results show that serpentine and iron oxide formed when olivine and orthopyroxene individually reacted with a saline starting solution. Olivine-derived serpentine had a significantly lower FeO content (6.57 ± 1.30 wt.%) than primary olivine (9.86 wt.%), whereas orthopyroxene-derived serpentine had a comparable FeO content (6.26 ± 0.58 wt.%) to that of primary orthopyroxene (6.24 wt.%). In experiments on peridotite, olivine was replaced by serpentine and iron oxide. However, pyroxene transformed solely to serpentine. After 20 days, olivine-derived serpentine had a FeO content of 8.18 ± 1.56 wt.%, which was significantly higher than that of serpentine produced in olivine-only experiments. By contrast, serpentine after orthopyroxene had a slightly higher FeO content (6.53 ± 1.01 wt.%) than primary orthopyroxene. Clinopyroxene-derived serpentine contained a significantly higher FeO content than its parent mineral. After 120 days, the FeO content of olivine-derived serpentine decreased significantly (5.71 ± 0.35 wt.%), whereas the FeO content of orthopyroxene-derived serpentine increased (6.85 ± 0.63 wt.%) over the same period. This suggests that iron oxide preferentially formed after olivine serpentinization. Pyroxene in peridotite gained some Fe from olivine during the serpentinization process, which may have led to a decrease in iron oxide production. The correlation between FeO content and SiO_2 or Al_2O_3 content in olivine- and orthopyroxene-derived serpentine indicates that aluminum and silica greatly control the production of iron oxide. Based on our results and data from natural serpentinites reported by other workers, we propose that aluminum may be more influential at the early stages of peridotite serpentinization when the production of iron oxide is very low, whereas silica may have a greater control on iron oxide production during the late stages instead.

1. Introduction

Serpentinization is a low-temperature (≤500 °C) hydrothermal alteration of ultramafic rocks (typically komatiite and peridotite), where olivine and pyroxene are hydrated to form serpentine, (±) brucite, and (±) magnetite (Eq. (1)):

* Corresponding author. Key Laboratory of Mineralogy and Metallogeny, Guangzhou Institute of Geochemistry, Chinese Academy of Sciences, Guangzhou 510640, PR China.
E-mail address: rfhuang@gig.ac.cn (R. Huang).
Peer-review under responsibility of China University of Geosciences (Beijing).

http://dx.doi.org/10.1016/j.gsf.2017.01.001

$$\underset{\text{olivine}}{(Mg_{1.8},Fe_{0.2})SiO_4} + 1.37H_2O = \underset{\text{serpentine}}{0.5Mg_3Si_2O_5(OH)_4} + \underset{\text{brucite}}{0.3Mg(OH)_2} + \underset{\text{magnetite}}{0.067Fe_3O_4} + 0.067H_2 \quad (1)$$

Serpentinization occurs in many geological settings on Earth, including the ocean floor, mid-ocean ridges and subduction zones (e.g., Charlou et al., 2002; Hyndman and Peacock, 2003; Mével, 2003; Evans et al., 2013). It dramatically modifies the physical, mechanical, and chemical properties of oceanic lithosphere (e.g., Escartín et al., 1997, 2001; Guillot and Hattori, 2013). Serpentinization leads to the uptake of voluminous H_2O (up to ~13 wt.%) and a dramatic decrease in density and strength (e.g., Escartín et al., 1997, 2001; Germanovich et al., 2012). Deformation experiments show that serpentine particularly lizardite is weaker than the other components of oceanic lithosphere, and a small degree of serpentinization (<15%) greatly reduces the strength of peridotite (Escartín et al., 1997, 2001). Moreover, serpentine can incorporate large quantities of fluid-mobile elements, such as B, Sr, and Cs (e.g., Hattori and Guillot, 2003; Scambelluri et al., 2004; Guillot and Hattori, 2013). Thermodynamic and experimental studies show that serpentine can remain stable at depths of greater than 150 km (Ulmer and Trommsdorff, 1995; Schmidt and Poli, 1998), suggesting that serpentinization is significant for the transfer of H_2O and fluid-mobile elements to the mantle.

Fluids derived from serpentinite-hosted hydrothermal fields typically contain abundant molecular hydrogen (H_2) and methane (CH_4), which can be utilized by communities of microorganisms to gain metabolic energy (e.g., Schrenk et al., 2004, 2013; Brazelton et al., 2006, 2010; Holm et al., 2015). Molecular hydrogen is produced by the oxidation of Fe^{2+} in olivine and pyroxene to Fe^{3+}. Ferric iron is mainly distributed into magnetite and silicate minerals (e.g., serpentine, talc, and tremolite). If all Fe^{3+} is incorporated into silicate minerals, magnetite may be absent during serpentinization (Seyfried et al., 2007; Evans, 2008; Evans et al., 2009).

However, the mechanisms that control H_2 production and the formation of magnetite are poorly understood (Bach et al., 2006; Beard et al., 2009; Frost et al., 2013). Analyses of serpentinized dunite and harzburgite suggest that magnetite is absent at the early stage of serpentinization when Mg-rich serpentine and Fe-rich brucite (around 27 wt.% FeO) form, whereas it is produced at the late stage of serpentinization through the breakdown of Fe-rich brucite (Bach et al., 2006). By contrast, Frost et al. (2013) argued that magnetite resulted from the extraction of iron from brucite and serpentine. However, the factors that control the distribution of iron between brucite and serpentine are poorly constrained. Based on the formation temperatures of serpentinites obtained according to oxygen isotopic compositions of serpentine minerals, Klein et al. (2014) proposed that magnetite is absent during serpentinization at temperatures below 200 °C. Consistently, experimental studies of peridotite serpentinization have shown that magnetite is not formed at 200 °C and 500 bar (Seyfried et al., 2007). By contrast, magnetite is produced at 200 °C after olivine serpentinization (McCollom et al., 2016), indicating that the process of magnetite formation during olivine serpentinization differs greatly from that during peridotite alteration. Compared to olivine, peridotite serpentinization produces one to two orders of magnitude more silica (e.g., Allen and Seyfried, 2003). Silica greatly controls the production of iron oxide during serpentinization, as it changes the composition and stability of Fe-bearing minerals (e.g., Bach et al., 2006; Frost and Beard, 2007; Klein et al., 2009). Frost and Beard (2007) reported that magnetite should theoretically be unstable at high silica activity. By contrast, analyses of natural serpentinites show that silica promotes magnetite production (Miyoshi et al., 2014). The controversy motivates us to investigate the influence of pyroxene and silica on magnetite production during serpentinization.

In this study, we performed serpentinization experiments at 311 °C and 3.0 kbar on natural ground orthopyroxene, olivine (with <5% pyroxene) and peridotite. Serpentinized harzburgite from the Lichi Mélange, Taiwan, was examined in order to compare with experimental observations in this study. This work aimed to (1) study the production of iron oxide during peridotite serpentinization, (2) illustrate the sequence of serpentinization reactions of olivine and orthopyroxene, and (3) study the influence of pyroxene on the formation of iron oxide during peridotite serpentinization.

2. Methods

2.1. Preparation of starting materials

The experimental strategy used in this study is to react olivine, orthopyroxene and spinel-bearing peridotite with a saline solution (0.5 mol/L NaCl). The peridotite was sampled at Panshishan (Jiangsu Province, China) where it occurs as xenoliths in alkaline basalts (Chen et al., 1994; Sun et al., 1998; Xu et al., 2008; Yang, 2008). It is composed of 60–65 vol.% olivine, 20–25 vol.% orthopyroxene, 15 vol.% clinopyroxene, and 1–2 vol.% spinel. The peridotite is fresh, as evidenced by a very small loss on ignition (typically less than 0.5%) upon heating at 1200 °C (Yang, 2008). Olivine and orthopyroxene were picked from crushed peridotite grains (<60 mesh) using a binocular microscope, and their fractions include less than 5% of other mineral phases. Peridotite, olivine and orthopyroxene were then ground in an agate mortar and sieved into a starting grain size of 100–177 μm. Small grains formed during crushing were removed with an ultrasonic bath. The starting fluid was prepared with fresh pure water and reagent-grade sodium chloride.

2.2. Preparation of gold capsules and experimental procedures

The solid reactants and starting solution were loaded into gold capsules (4.0 mm outer diameter, 0.2 mm wall thickness, and 30 mm long). The water/rock ratios, *i.e.*, mass ratios between the starting solution and the solid reactants, are ~1.0. Gold is commonly used in serpentinization experiments (e.g., Berndt et al., 1996; Malvoisin et al., 2012) because it is chemically inert and does not form any Fe-Au alloy at low temperatures (e.g., ≤500 °C). The capsules were double-sided welded with a tungsten inert gas high-frequency pulse welder (PUK3). Leaks were checked before and after all experiments by putting capsules in a drying furnace at 100 °C for at least 2 h. Only capsules with mass differences less than 0.5% from the initial mass before heating were used in experiments.

All experiments were performed in cold-seal hydrothermal vessels at the Guangzhou Institute of Geochemistry, Chinese Academy of Sciences (Table 1). The capsules were loaded into the end of hydrothermal vessels, followed with a filler rod (~6 cm in

Table 1
Experimental conditions.

Sample No.	Starting material	Water/rock ratios[a]	Time (days)	Products
Fe37	Olivine	1.1	26	Srp, Mgt, Ol
HR42	Orthopyroxene	0.82	18	Srp, Opx
HR25	Peridotite	1.4	19	Srp, Mgt, Ol, Opx, Cpx
HR61	Peridotite	0.82	120	Srp, Mgt, Ol, Opx, Cpx
HR77	Peridotite	1.2	28	Srp, Mgt, Ol, Opx, Cpx

[a] Mass ratios between the starting solution and the solid reactant loaded into gold capsules.

length). Pressures were achieved by pumping water into the vessel and were measured by a pressure gauge with a precision of ±100 bar. Temperatures were monitored with an external K-type thermocouple that was inserted into a hole near the end of the vessel, which had an accuracy of ±2 °C. When finished, the vessels were chilled by immersion into ice water, whereby the temperatures of gold capsules decreased to <100 °C within a few seconds.

2.3. Analytical methods

Following these experiments, each capsule was pierced by a tungsten needle, and was dried at 70 °C for at least 24 h. The surface morphology of solid products was characterized by secondary electrons using a Zeiss Ultra 55 field emission gun scanning electron microscope (FESEM). Samples were dispersed onto double-sided carbon tape and coated with a thin film of platinum for FESEM observations.

The mineralogy of solid products was identified with a Bruker Vector 33 Fourier transform infrared spectrometer at the Analytical and Testing Center of South China University of Technology. Infrared spectra were obtained at wavenumbers from 400 to 4000 cm^{-1} at a resolution of 4 cm^{-1}, and 32 scans were accumulated for each spectrum. The KBr pellets were prepared by mixing ~1 mg of sample powder with 200 mg of KBr.

The chemical compositions of solid run products were analyzed with a JEOL JXA 8100 electron microprobe at the Second Institute of Oceanography, State Oceanic Administration of China. Operating conditions for serpentine analyses included 15 kV and 20 nA with a beam diameter of 15 μm. Calibration standards were jadeite (Si, Na), olivine (Mg), almandine garnet (Fe, Al), diopside (Ca), sandine (K), chromium oxide (Cr), rutile (Ti), nickel silicide (Ni), rhodonite (Mn), and tugtupite (Cl). The counting time for Ni, Co, Mn, Cr, and Cl was 30 s for peak and 10 s for background, whereas other elements were analyzed with 10 s for peak and 5 s for background.

3. Results and discussions

3.1. Identification of secondary minerals

The main secondary hydrous mineral produced in our experiments was fibrous chrysotile (Fig. 1a, b). Infrared spectra of solid products show bands typical of serpentine at 954, 1087, and 3686 cm^{-1} (Fig. 1c). The bands at 954 and 1087 cm^{-1} represent stretching modes of the Si–O group in serpentine, and that at 3686 cm^{-1} represents a stretching vibration of the –OH group (e.g., Anbalagan et al., 2010; Lafay et al., 2014). The electron microprobe-derived chemical compositions of solid products confirmed that the main secondary hydrous mineral produced in our runs was serpentine (Table 2).

Brucite was not produced in any of our experiments. The stability of brucite depends strongly on temperature and silica activity (Bach et al., 2006; McCollom and Bach, 2009; Marcaillou et al., 2011). Thermodynamic modeling indicates that the stability of brucite decreases significantly with increasing temperature, and

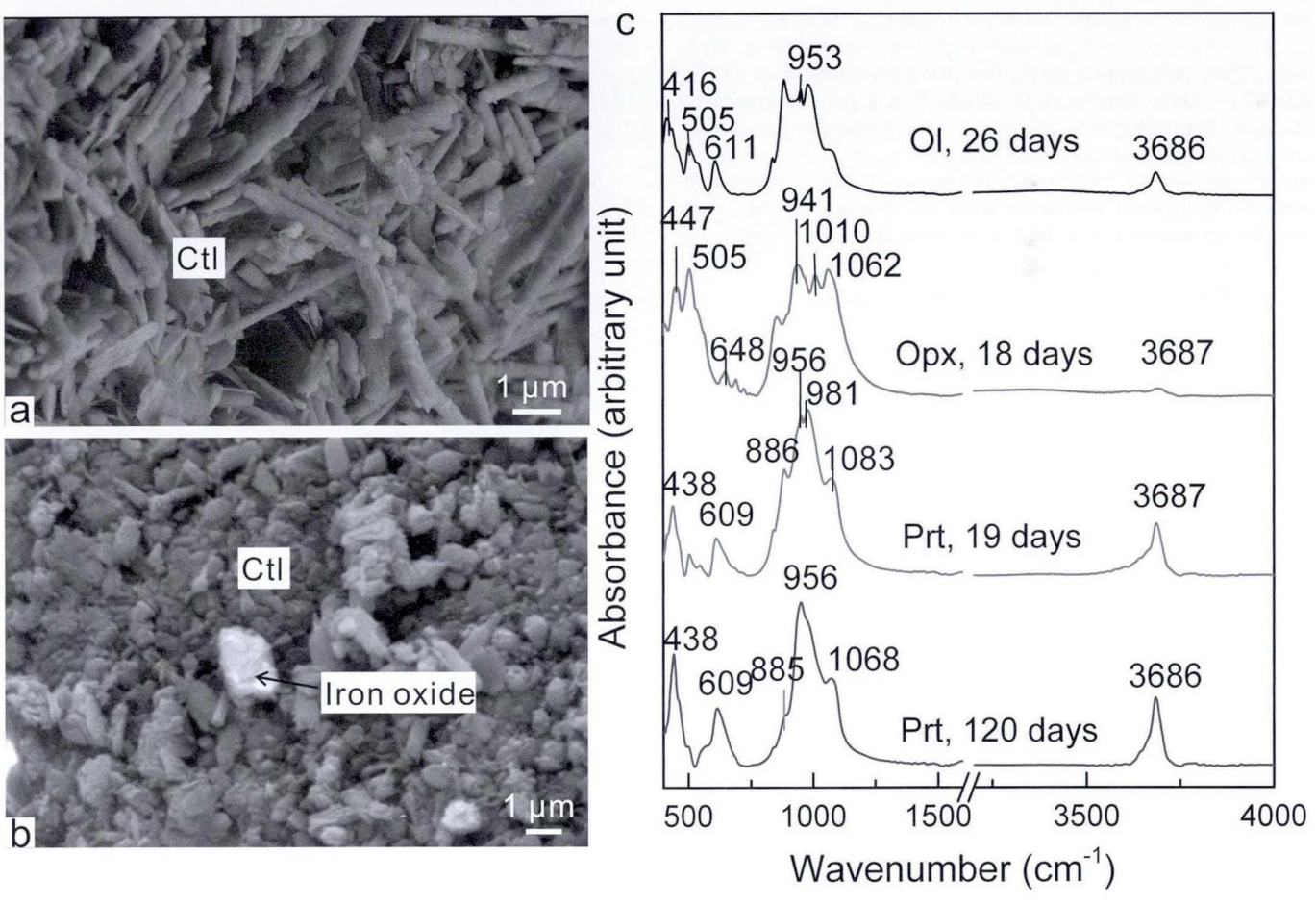

Figure 1. Identification of solid products based on scanning electron microscope images and Fourier transform infrared spectra. (a) HR61, with peridotite as starting material. Fibrous chrysotile was formed. (b) Fe37, with olivine as starting material. Fibrous chrysotile and iron oxide were produced. (c) Infrared spectra of solid products, showing that serpentine was the main secondary hydrous mineral.

Table 2
Chemical compositions of serpentine produced in experiments.

Sample No.	SiO_2	TiO_2	Cr_2O_3	Al_2O_3	MgO	FeO	CaO	MnO	NiO	K_2O	Na_2O	Cl	Total	Minerals[a]
HR25-34	40.74	–	0.00	3.19	36.91	4.05	0.11	0.16	0.51	0.04	0.26	0.04	86.02	Opx
HR25-35	40.32	–	0.05	3.45	37.10	4.56	0.14	0.11	0.24	0.03	0.20	0.07	86.31	Opx
HR25-36	39.89	0.05	0.17	3.49	35.91	5.20	0.19	0.13	0.17	0.04	0.17	0.22	85.66	Opx
HR25-37	40.65	–	0.43	1.68	37.13	6.82	0.02	0.10	0.12	0.00	0.07	0.06	87.08	Opx
HR25-29	40.58	0.01	0.03	0.61	39.42	6.82	0.07	0.09	0.40	0.01	0.19	0.13	88.39	Ol
HR25-30	39.35	0.10	0.04	2.42	34.95	8.81	0.10	0.10	0.24	0.01	0.19	0.10	86.42	Ol
HR25-31	39.82	0.02	0.04	2.87	35.63	9.63	0.06	0.05	0.32	0.02	0.12	0.05	88.62	Ol
HR25-32	39.67	–	0.01	3.02	35.75	8.94	0.08	0.10	0.31	0.01	0.14	0.11	88.14	Ol
HR61-2	39.08	0.01	0.00	1.27	35.89	5.14	0.05	0.06	0.34	0.00	0.06	0.06	81.95	Ol
HR61-3	39.02	0.00	0.00	1.18	35.74	5.43	0.05	0.06	0.51	0.01	0.05	0.07	82.11	Ol
HR61-4	39.63	0.00	0.02	1.18	36.31	5.76	0.04	0.01	0.54	0.00	0.05	0.03	83.57	Ol
HR61-6	39.30	0.00	0.02	1.40	36.28	5.32	0.06	0.07	0.42	0.01	0.04	0.07	82.99	Ol
HR61-11	39.69	0.04	0.02	1.43	35.79	5.06	0.04	0.04	0.38	0.00	0.06	0.07	82.60	Ol
HR61-16	39.47	0.02	0.06	1.29	35.80	6.01	0.10	0.06	0.46	0.00	0.03	0.11	83.39	Ol
HR61-18	37.92	0.06	0.51	1.64	35.18	6.21	0.61	0.08	0.07	0.01	0.15	0.19	82.58	Opx
HR61-19	38.10	0.08	0.46	1.77	35.58	6.44	0.25	0.14	0.15	0.01	0.15	0.13	83.23	Opx
HR61-20	38.43	0.05	0.47	1.79	35.76	6.38	0.24	0.08	0.08	0.00	0.19	0.19	83.61	Opx
HR61-21	38.55	0.08	0.45	1.79	35.21	6.28	0.24	0.11	0.14	0.00	0.21	0.24	83.26	Opx
Fe37-11	36.88	0.06	0.09	3.56	36.01	5.12	0.07	0.06	0.10	0.01	0.09	0.19	82.18	Ol
Fe37-13	38.27	0.00	0.06	0.70	38.94	7.23	0.10	0.05	0.39	0.00	0.09	0.08	85.89	Ol
Fe37-1	36.94	0.02	0.03	3.47	33.85	7.86	0.11	0.03	0.33	0.00	0.04	0.06	82.72	Ol
Fe37-3	37.96	0.00	0.00	4.02	34.40	7.10	0.10	0.09	0.29	0.03	0.03	0.03	84.03	Ol
HR42-87	43.22	0.07	0.23	2.72	32.48	6.63	0.79	0.11	0.11	0.01	0.17	0.77	87.13	Opx
HR42-88	43.32	0.03	0.22	2.69	32.10	6.41	1.27	0.15	0.09	0.02	0.16	0.77	87.05	Opx
HR42-89	42.62	0.06	0.23	2.63	31.66	6.41	0.81	0.26	0.10	0.01	0.14	0.69	85.49	Opx
HR42-90	38.16	0.08	0.12	7.56	32.94	6.21	0.17	0.07	0.04	0.04	0.10	0.06	85.54	Opx

[a] Parent minerals of serpentine. Ol: olivine, Opx: orthopyroxene.

almost none is produced at temperatures above 310 °C (McCollom and Bach, 2009). Moreover, brucite is unstable at high silica activities as it reacts with SiO_2 to form serpentine minerals (e.g., Bach et al., 2006). Consistently, serpentinization experiments at 300 °C and 500 bar show that brucite is absent during peridotite serpentinization (Marcaillou et al., 2011). Additionally, brucite production can be strongly influenced by reaction time, e.g., brucite is absent in experiments with a short run duration (~75 days), whereas it forms in experiments conducted at the same conditions but with much longer reaction time (McCollom et al., 2016).

3.2. Chemical compositions of serpentine minerals

When olivine and orthopyroxene reacted individually with the starting solution, they were replaced by serpentine and iron oxide (Fig. 2a, b). The iron oxide produced typically has a very small grain size (~1 μm). Serpentine that replaced olivine had a much lower FeO content (6.57 ± 1.30 wt.%) than that of primary olivine (9.86 wt.%), whereas serpentine minerals that replaced orthopyroxene contained identical FeO contents (6.26 ± 0.58 wt.%) to those of primary grains (6.24 wt.% FeO). By contrast, in experiments with peridotite, olivine was hydrated to form serpentine and iron oxide (Fig. 2c), but orthopyroxene was replaced solely by serpentine (Fig. 2d). After an experimental duration of 20 days, olivine-derived serpentine had 8.18 ± 1.56 wt.% FeO, slightly lower than the FeO content of primary olivine (Fig. 3a), but significantly higher than that of serpentine formed in olivine-only experiments (Table 2). Orthopyroxene-derived serpentine had a slightly higher FeO content (6.53 ± 1.01 wt.%) than that of primary orthopyroxene, and serpentine that replaced clinopyroxene had 7.23 ± 0.61 wt.% FeO, which was significantly higher than the FeO content of primary clinopyroxene (2.61 wt.%).

After an experimental duration of 120 days, the FeO contents in olivine-derived serpentine decreased significantly (5.71 ± 0.35 wt.%) compared to those produced after 20 days (Fig. 3a, Table 2). By contrast, the FeO contents of serpentine after orthopyroxene slightly increased to 6.85 ± 0.63 wt.% over this period, which suggests that iron oxide formed via the extraction of iron from early-formed serpentine or directly as a result of olivine serpentinization. Pyroxene obtained more iron from olivine with progressive serpentinization, which resulted in the production of Fe-rich serpentine, and likely caused a commensurate decrease in iron oxide production.

3.3. Sequence of the hydration of olivine and orthopyroxene during peridotite serpentinization

Based on scanning electron microscope images and chemical compositions of serpentine, we propose the following sequence of reactions for the hydration of olivine and orthopyroxene in experiments on peridotite. First, olivine was hydrated to form serpentine and a few dispersed iron oxide minerals (Eq. (2)).

$$\underset{\text{olivine}}{(Mg_{1.8},Fe_{0.2})SiO_4} + 0.33SiO_2 + 1.33H_2O = \underset{\text{serpentine}}{0.66(Mg_{2.71},Fe_{0.29})Si_2O_5(OH)_4} + \underset{\text{magnetite}}{0.0025Fe_3O_4} + 0.002H_2 \quad (2)$$

Serpentine had a slightly lower FeO content than primary olivine. Iron was mostly incorporated into serpentine as Fe^{2+} or Fe^{3+}. By contrast, orthopyroxene was replaced by serpentine minerals that contained identical iron contents to those of primary orthopyroxene (Eq. (3)). Iron was distributed into orthopyroxene-derived serpentine mostly as Fe^{2+}, as almost no Fe^{2+} within orthopyroxene was oxidized into Fe^{3+}, due to the absence of iron oxide.

$$\underset{\text{orthopyroxene}}{(Mg_{1.7}\cdot Fe_{0.18})(Al_{0.2},Si_{1.9})O_6} + 2H_2O = \underset{\text{serpentine}}{(Mg_{2.71}\cdot Fe_{0.29})(Al_{0.2},Si_{1.9})O_5(OH)_4} \quad (3)$$

With continued serpentinization, the Fe in olivine-replaced serpentine was extracted and then oxidized, which produced

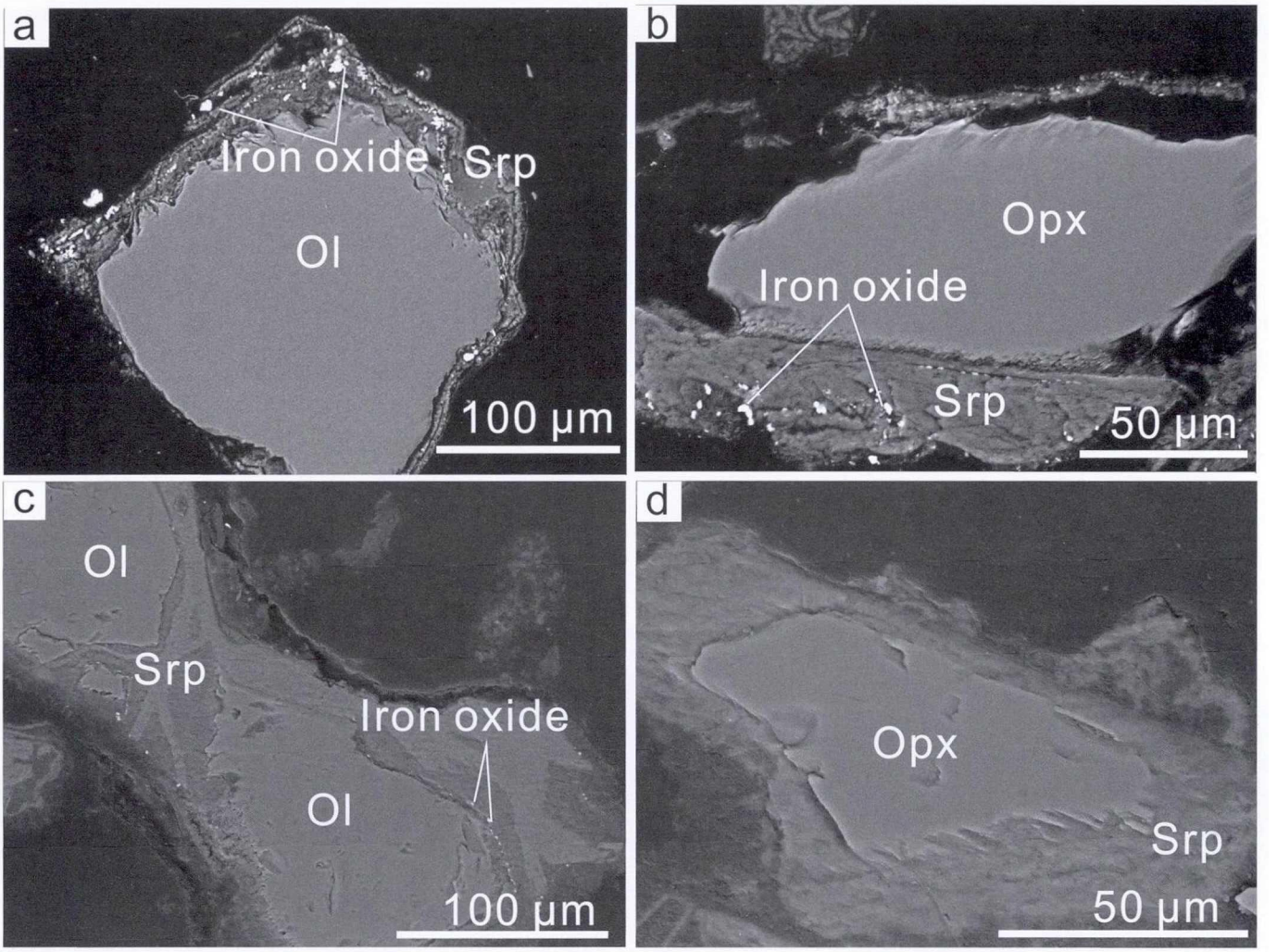

Figure 2. Backscattered electron images of experimental run products. (a) Fe37, olivine was replaced by serpentine and iron oxide. (b) HR42, orthopyroxene was hydrated to serpentine and iron oxide. (c) HR25, with peridotite as starting material. Olivine transformed into serpentine and a few dispersed iron oxide. (d) HR25, orthopyroxene alteration produced serpentine without forming any iron oxide.

relatively Fe-poor serpentine and additional iron oxide minerals. By contrast, orthopyroxene obtained some Fe from olivine during serpentinization, which led to an increase in the FeO content of serpentine that replaced orthopyroxene.

3.4. *Influence of pyroxene on the formation of iron oxide during serpentinization*

Previous experiments show that magnetite production during olivine serpentinization increases linearly with reaction progress (Malvoisin et al., 2012), whereas it has an exponential correlation with reaction progress during peridotite serpentinization (Toft et al., 1990; Oufi et al., 2002; Bach et al., 2006; Marcaillou et al., 2011). It suggests that iron oxide production during olivine serpentinization differs greatly from that after peridotite alteration, possibly resulting from the presence of pyroxene minerals. Previous experiments show that magnetite preferentially forms in olivine-bearing zones, whereas it is absent at olivine/orthopyroxene interfaces (Ogasawara et al., 2013). The absence of magnetite after orthopyroxene serpentinization has also been reported in naturally serpentinized peridotite (Rouméjon et al., 2015). As demonstrated by experiments in this study, pyroxene minerals obtained some iron from olivine during peridotite serpentinization, and serpentine formed from orthopyroxene and clinopyroxene was more enriched in FeO than its hosts, which may lead to a decrease in the production of iron oxide.

Pyroxene minerals release some of its aluminum during serpentinization, which may greatly control the production of iron oxide. Although fluids derived from serpentinization typically have very low Al concentrations (e.g., Okamoto et al., 2011), aluminum is at least locally mobile, supported by the following evidence. First, chemical compositions analyzed with electron microprobe show that olivine-derived serpentine formed in experiments on peridotite had a much higher Al_2O_3 content than primary olivine, whereas pyroxene-derived serpentine contained a significantly lower Al_2O_3 content than its hosts (Fig. 3b), indicating releases of aluminum from pyroxene minerals. Moreover, the Al_2O_3 content of olivine-derived serpentine was largely scattered (1.89 ± 1.26 wt.%) after an experimental duration of 20 days, and it became more homogenous after longer reaction time (1.67 ± 0.1 wt.%, 120 days), indicating that aluminum is mobile. Analyses of natural serpentinites also show that orthopyroxene loses ~50% of its aluminum to neighboring olivine during serpentinization (e.g., Dungan, 1979; Hébert et al., 1990). As illustrated in Fig. 4a, the Al_2O_3 contents in olivine-derived serpentine produced in experiments on peridotite with reaction time of 20 days were positively correlated with the

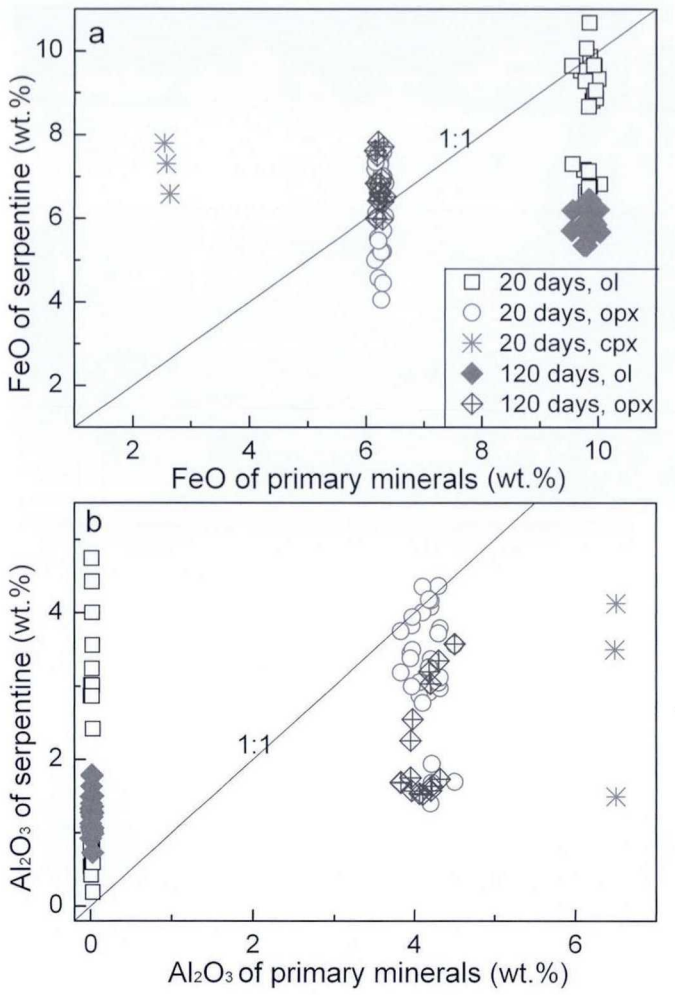

Figure 3. (a) Partitioning of iron between serpentine and its parent minerals (olivine and pyroxene). When run durations were increased from 20 to 120 days, the FeO contents of olivine-derived serpentine decreased significantly, while those of orthopyroxene-derived serpentine increased slightly. This indicates that iron oxide was formed during olivine serpentinization, and that pyroxene minerals obtained some iron from olivine during peridotite serpentinization, possibly resulting in a decrease in iron oxide production. (b) Partitioning of aluminum between serpentine and its hosts (olivine and pyroxene). Olivine-derived serpentine had a significantly higher Al_2O_3 content than primary olivine, whereas pyroxene-derived serpentine contained a much lower Al_2O_3 content than its parent minerals, indicating releases of aluminum from pyroxene minerals.

FeO contents. Releases of aluminum from pyroxene minerals could increase the Al_2O_3 contents of olivine-derived serpentine, which may raise its FeO contents. Consequently, the production of iron oxide possibly decreases, as iron is mainly incorporated into serpentine and iron oxide. The influence of aluminum was also supported by experimental results of Andreani et al. (2013), which showed that magnetite was not produced with the addition of abundant aluminum during olivine serpentinization. By contrast, the Al_2O_3 contents of orthopyroxene-derived serpentine were negatively correlated with the FeO contents (Fig. 4b). Release of aluminum from orthopyroxene resulted in the formation of Al-deficient serpentine, possibly leading to an increase in the FeO content of orthopyroxene-derived serpentine and a decrease in iron oxide production. However, there was no correlation between Al_2O_3 and FeO contents of olivine-derived serpentine formed after a longer experimental duration, possibly due to very homogenous Al_2O_3 and FeO contents (Fig. 4c), whereas the negative correlation between Al_2O_3 and FeO contents of orthopyroxene-derived serpentine was still detected (Fig. 4d).

Pyroxene minerals release some of its silica during serpentinization, which strongly influence iron oxide production. Experiments show that peridotite serpentinization produces dissolved SiO_2 around one order of magnitude higher than that formed during olivine serpentinization (e.g., Seyfried and Dibble, 1980; Allen and Seyfried, 2003). As suggested by Frost and Beard (2007), magnetite forms from the oxidation of Fe^{2+}-serpentine (Eq. (4)), and it is not stable at high silica activity.

$$\underset{\text{serpentine}}{2Fe_3Si_2O_5(OH)_4} + O_2 = \underset{\text{magnetite}}{2Fe_3O_4} + 4SiO_{2,aq} + 4H_2O \quad (4)$$

By contrast, Miyoshi et al. (2014) proposed that silica promotes magnetite production, based on their observations that (1) the magnetic susceptibility of serpentinized harzburgite was linearly correlated with the degree of serpentinization, and (2) such correlation was not identified for serpentinized dunite that had a much lower magnetic susceptibility. However, experiments conducted on olivine serpentinization have shown that magnetite production has a linear relationship with reaction progress (e.g., Malvoisin et al., 2012). It is possibly because magnetic susceptibility greatly depends on crystal shapes and the grain size distribution of magnetite (e.g., Fukuma and Dunlop, 2006; Ge and Liu, 2014). Magnetic susceptibility decreases by one order of magnitude when the grain size of magnetite increases from 0.03 to 0.3 μm (e.g., Fukuma and Dunlop, 2006). As magnetite in serpentinites typically has a wide variation in grain size, there are large uncertainties associated with magnetic susceptibility and the amounts of magnetite produced.

Serpentine produced in our orthopyroxene-only experiments had 42.9 ± 0.72 wt.% SiO_2, which was significantly higher than the SiO_2 content of serpentine produced in olivine-only experiments (37.1 ± 1.7 wt.%). By contrast, orthopyroxene-derived serpentine produced in experiments on peridotite with a run duration of 20 days had comparable SiO_2 contents (39.7 ± 0.7 wt.%) with serpentine after olivine (39.3 ± 1.1 wt.% SiO_2). After an experimental duration of 120 days, the SiO_2 contents of serpentine that replaced orthopyroxene decreased greatly, whereas the SiO_2 contents of serpentine that replaced olivine increased (Fig. 5). All these indicate that orthopyroxene lost some of its SiO_2 to neighboring olivine during serpentinization, and that silica is mobile. The mobility of silica has been reported in Malvoisin (2015), based on geochemical dataset of serpentinized peridotite at mid-ocean ridges. Fig. 5 shows that the measured SiO_2 contents in olivine-derived serpentine were inversely correlated with their FeO contents. The release of SiO_2 from pyroxene caused an increase in the SiO_2 contents of olivine-derived serpentine, which may lead to a decrease in the FeO contents. Consequently, the production of iron oxide possibly increased. Based on our results and previous studies (Toft et al., 1990; Oufi et al., 2002; Bach et al., 2006; Marcaillou et al., 2011), we propose that aluminum may be more influential at the early stage of serpentinization (reaction extents less than 75%) when magnetite production is very low. It is also supported by the production of iron oxide in our orthopyroxene-only experiments and the absence of iron oxide after orthopyroxene alteration in experiments on peridotite. However, silica may greatly control the production of iron oxide at the late stage of serpentinization.

3.5. Comparison with natural samples

To compare with the experimental results in this study, we studied serpentinized harzburgite from the Lichi Mélange, Taiwan (TA-1: N23°02′14.3″, E121°12′1.5″; DX-1: N23°01′15.5″,

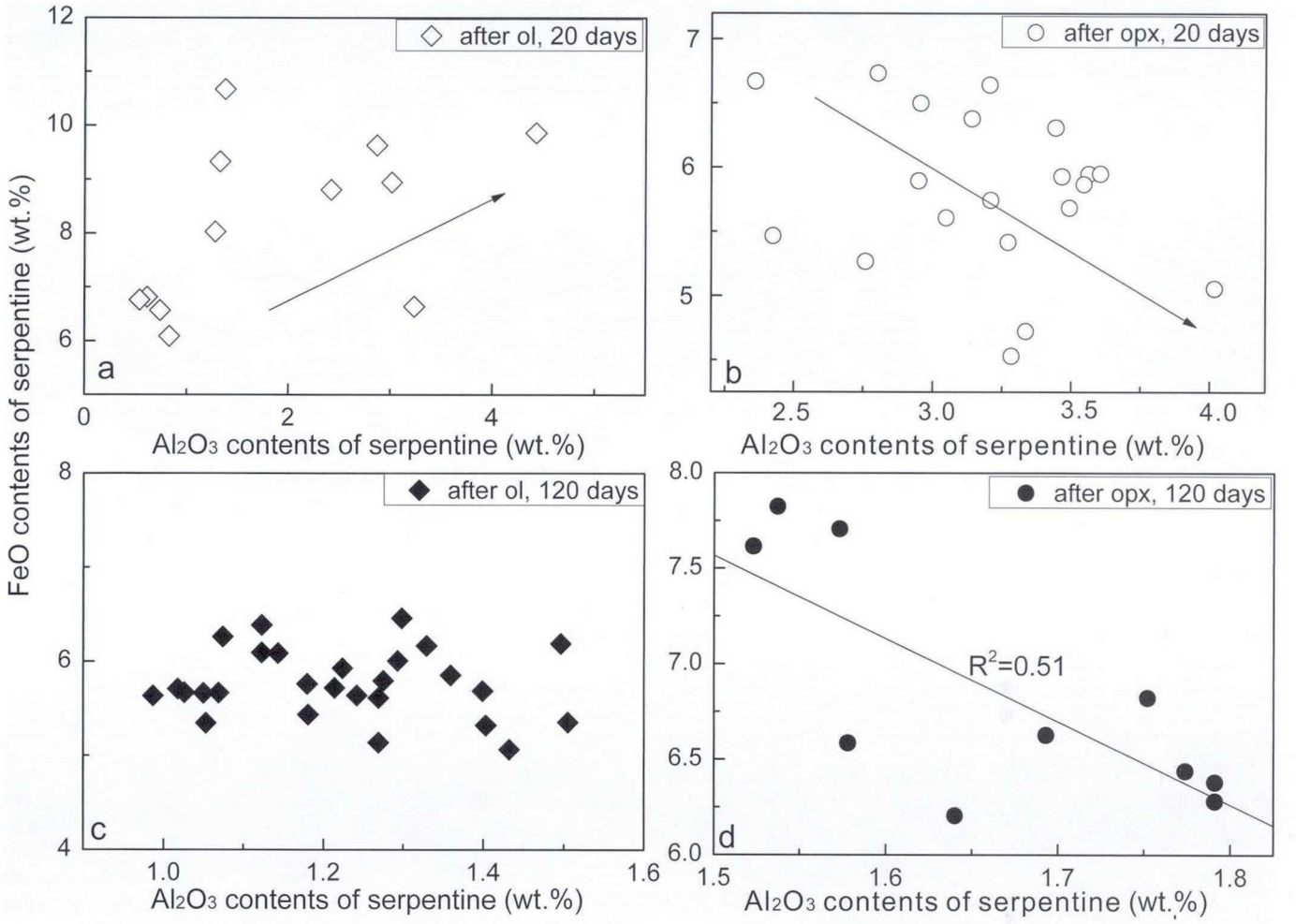

Figure 4. The correlation between FeO (wt.%) and Al_2O_3 contents (wt.%) in olivine- and orthopyroxene-derived serpentine minerals.

E121°11′37.0″; and JWN-1: N23°01′51.6″, E121°11′41.6″). Harzburgite was completely replaced by serpentinite, but the pseudomorphs of olivine and orthopyroxene have been preserved (Fig. 6). The precursor minerals of serpentine were identified based on the distinct chemical compositions of serpentine after olivine and pyroxene (Fig. 7). Previous studies show that serpentine derived from pyroxene alteration has significantly more Al and Cr than serpentine after olivine (e.g., Dungan, 1979; Hébert et al., 1990; Huang et al., 2015a). Raman spectroscopy analyses show that both magnetite and hematite occur in serpentinites. All iron oxide observed in these samples was distributed around olivine pseudomorphs, whereas it was absent around pyroxene pseudomorphs (Fig. 6). Dispersed iron oxide in serpentine was not observed, but it was formed after olivine serpentinization in our experiments on peridotite. It implies that iron is at least locally mobile, and that dissolution and reprecipitation of iron oxide can commonly occur during serpentinization.

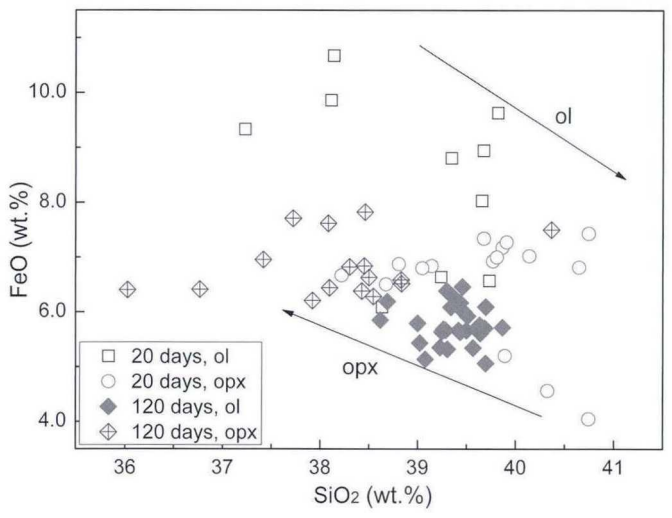

Figure 5. Silica and FeO contents (wt.%) of serpentine minerals formed from olivine and orthopyroxene. ol–olivine; opx–orthopyroxene.

In order to illustrate the influence of silica mobility on the FeO content of serpentine, we studied breccias from the Lichi Mélange, Taiwan. The breccias are composed of serpentinized fragments of minerals (olivine and orthopyroxene) and a fine-grained matrix (Fig. 8a). Olivine and orthopyroxene have largely varied grain sizes, ranging from ~10 to 500 μm. Serpentine that replaced small-sized olivine and orthopyroxene (e.g., ~20 μm) had abundant SiO_2 (~42 wt.%) whereas serpentine that replaced olivine and orthopyroxene with larger grain sizes (e.g., ≥200 μm) contained much lower SiO_2 content (~39 wt.%, Fig. 8b). Analyses along transects of completely serpentinized primary minerals (~400 μm) show that SiO_2 is homogenously distributed (Fig. 9), indicating that the incorporation of SiO_2 into serpentine is not through diffusion.

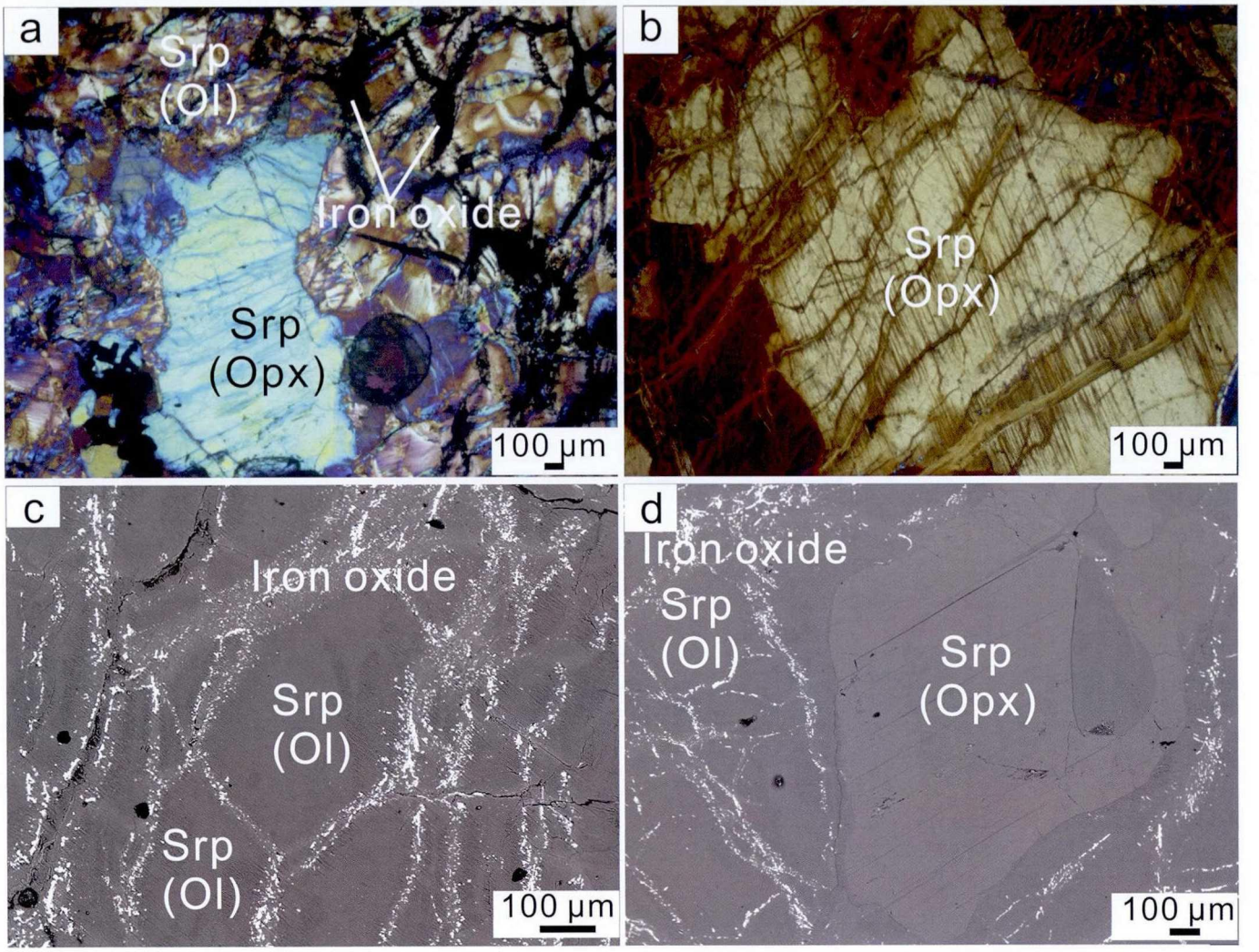

Figure 6. Optical and backscattered electron images of serpentinized harzburgite from the Lichi Mélange, Taiwan. It shows that all iron oxide was distributed around olivine pseudomorphs, and it was absent around orthopyroxene pseudomorphs. Srp (Ol), olivine-derived serpentine; Srp (Opx), orthopyroxene-derived serpentine.

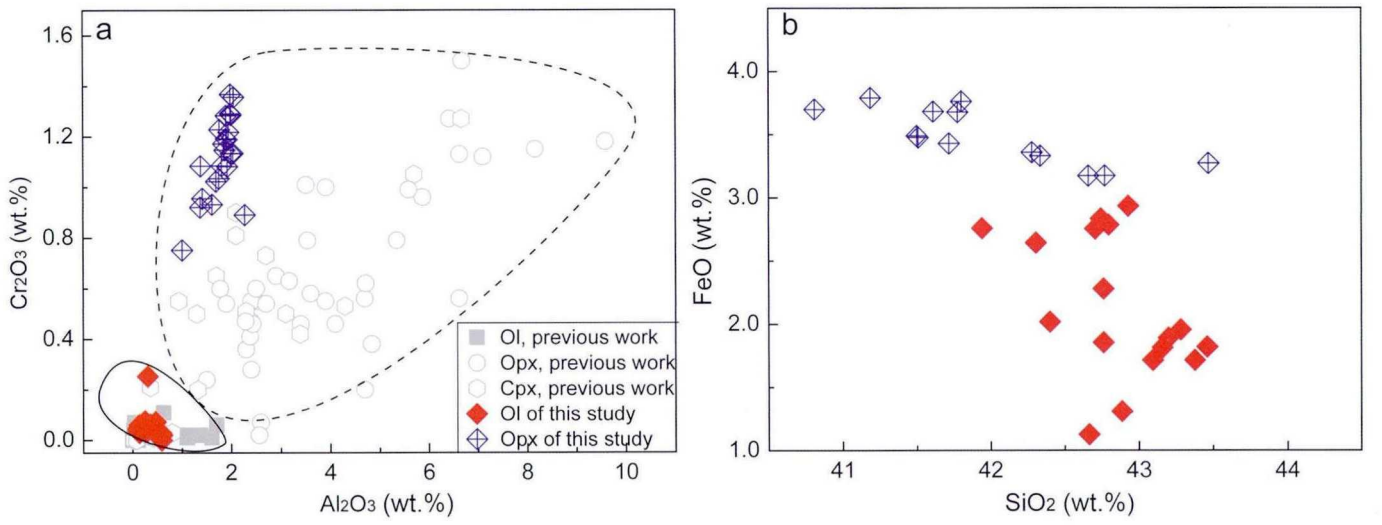

Figure 7. (a) Discrimination diagram for serpentine minerals formed from olivine or pyroxene. Gray-colored background data are from Dungan (1979) and Hébert et al. (1990). Serpentine that replaced pyroxene was more enriched in Al and Cr compared to that replaced olivine. (b) FeO and SiO_2 contents of olivine- and orthopyroxene-derived serpentine minerals in hydrated harzburgite from the Lichi Mélange, Taiwan.

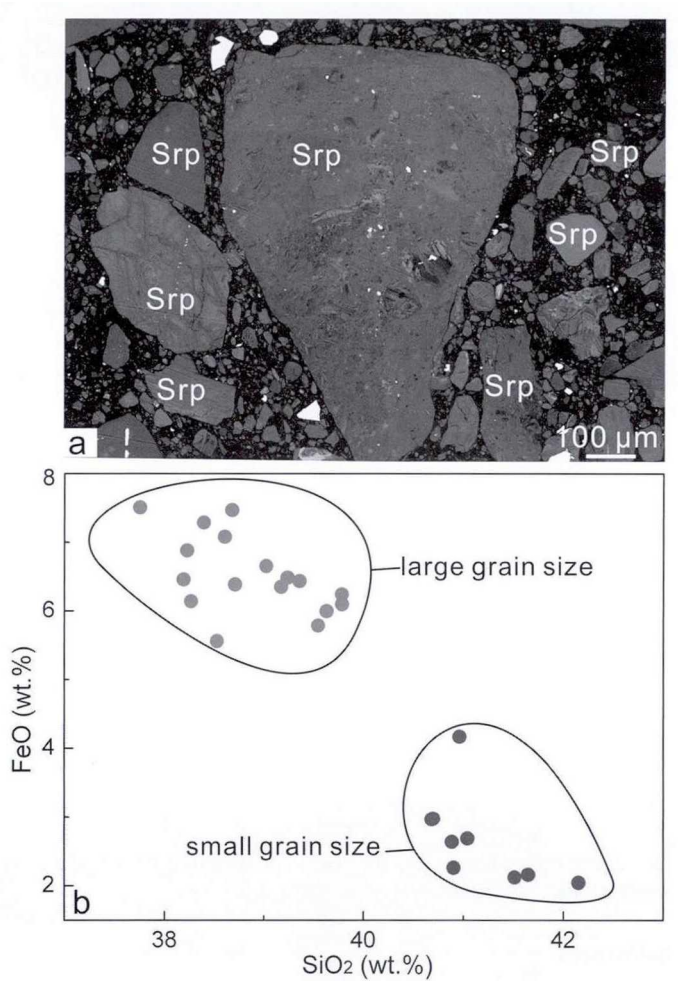

Figure 8. (a) Backscattered electron images of breccias with serpentinized fragments of minerals (olivine and orthopyroxene) and a fine-grained matrix from the Lichi Mélange, Taiwan. (b) The negative correlation between FeO contents (wt.%) and SiO_2 contents (wt.%) of serpentine from the breccias. It shows that the SiO_2 contents of serpentine strongly depend on the grain size of its parent minerals. Serpentine that replaced small-sized olivine and orthopyroxene (e.g., ~20 μm) had abundant SiO_2 (~42 wt.%) whereas serpentine that replaced olivine and orthopyroxene with larger grain sizes (e.g., ≥200 μm) contained much lower SiO_2 contents (~39 wt.%).

Otherwise, chemical gradients should be produced. The FeO contents of serpentine minerals were negatively correlated with their SiO_2 contents (Fig. 8b). The release of silica from fine-grained matrix during hydrothermal alteration may increase the SiO_2 content of serpentine minerals, possibly resulting in a decrease in their FeO contents, consistent with experimental results of this study. However, the correlation between FeO and SiO_2 contents may not be always detected, e.g., Evans (2008) found that the FeO contents of serpentine formed during dunite serpentinization are essentially the same as those of serpentine formed in the vicinity of orthopyroxene. It is possibly because the distribution of iron between serpentine minerals and iron oxide can be strongly influenced by many factors, such as temperature (e.g., McCollom and Bach, 2009; Evans, 2010; Müntener, 2010; Klein et al., 2014), the pH and CO_2 contents in the starting fluids (Lafay et al., 2012, 2014; Holm et al., 2015), and water/rock ratios (McCollom and Bach, 2009).

3.6. Geological implications

This study suggests that iron oxide formed during peridotite serpentinization results from the oxidation of ferrous iron in olivine into ferric iron, whereas the presence of pyroxene minerals impedes the production of iron oxide, due to releases of aluminum and silica. In natural geological settings, olivine is typically intimately associated with Al_2O_3, SiO_2-supplier such as pyroxene, plagioclase and amphibole, and consequently the production of iron oxide can be greatly influenced. The formation of iron oxide during serpentinization is closely associated with H_2 production, implying that aluminum and silica could affect H_2 formation. Indeed, previous experiments suggest that peridotite serpentinization produces significantly larger quantities of H_2 and CH_4 than olivine hydration (Huang et al., 2015b), possibly resulting from releases of aluminum from pyroxene and spinel. The influence of aluminum on H_2 production in a natural system has been described by Seyfried et al. (2011), based on fluid compositions in Rainbow hydrothermal field (36°N, Mid-Atlantic Ridge). By contrast, thermodynamic modeling indicates that silica decreases the production of H_2 (Seyfried et al., 2011).

Releases of aluminum and silica from Al_2O_3, SiO_2-supplier (e.g., plagioclase, pyroxene and amphibole) may greatly depend on temperature and water/rocks ratios (e.g., Allen and Seyfried, 2003; McCollom and Bach, 2009). Thermodynamic modeling shows that the amounts of dissolved SiO_2 in fluids increase at higher temperatures, whereas they decrease greatly at higher water/rock ratios (e.g., McCollom and Bach, 2009). As reported by Andreani et al. (2013), almost no aluminum was released from Al_2O_3 powders at temperatures of ≤200 °C, whereas releases of aluminum were detected at higher temperatures (e.g., 300 °C). By contrast, serpentinization experiments at 80–200 °C and vapor saturated pressures show that olivine-derived serpentine has significantly higher Al_2O_3 contents than primary olivine, whereas pyroxene-derived serpentine contains much lower Al_2O_3 contents than its hosts (Huang et al., 2015a), indicating releases of aluminum from pyroxene minerals. It also indicates that pyroxene is an important source of aluminum during serpentinization.

This study suggests that iron oxide production during serpentinization is strongly influenced by Al_2O_3 and SiO_2 contents of serpentine, based on the correlation between FeO and Al_2O_3 or SiO_2 contents of serpentine minerals. Moreover, the Al_2O_3 and SiO_2 contents of serpentine greatly control the distribution of chlorine into serpentine. Analyses of natural serpentinites show that serpentine formed after olivine has much lower chlorine contents than serpentine after orthopyroxene, and chlorine in orthopyroxene-derived serpentine is positively correlated with Al_2O_3 but negatively correlated with SiO_2 (Bonifacie et al., 2008). It indicates that aluminum and silica influence the distribution of other structurally-bound elements into serpentine minerals.

4. Conclusions

In this study, we performed serpentinization experiments at 311 °C and 3.0 kbar on olivine (<5% pyroxene minerals), orthopyroxene, and peridotite. Serpentine minerals and iron oxide were formed when olivine and orthopyroxene individually reacted with a saline starting fluid. By contrast, olivine was replaced by serpentine minerals and iron oxide in experiments on peridotite, whereas orthopyroxene transformed into serpentine. After an experimental duration of 20 days, olivine-derived serpentine had significantly higher FeO contents than serpentine produced in experiments on olivine. By contrast, orthopyroxene-derived serpentine contained higher FeO contents than that formed in experiments on orthopyroxene. After 120 days, the FeO contents in serpentine after olivine decreased greatly, whereas the FeO contents in serpentine after orthopyroxene increased slightly. It suggests that iron oxide forms via the extraction of iron from early-formed serpentine or directly as a result of olivine

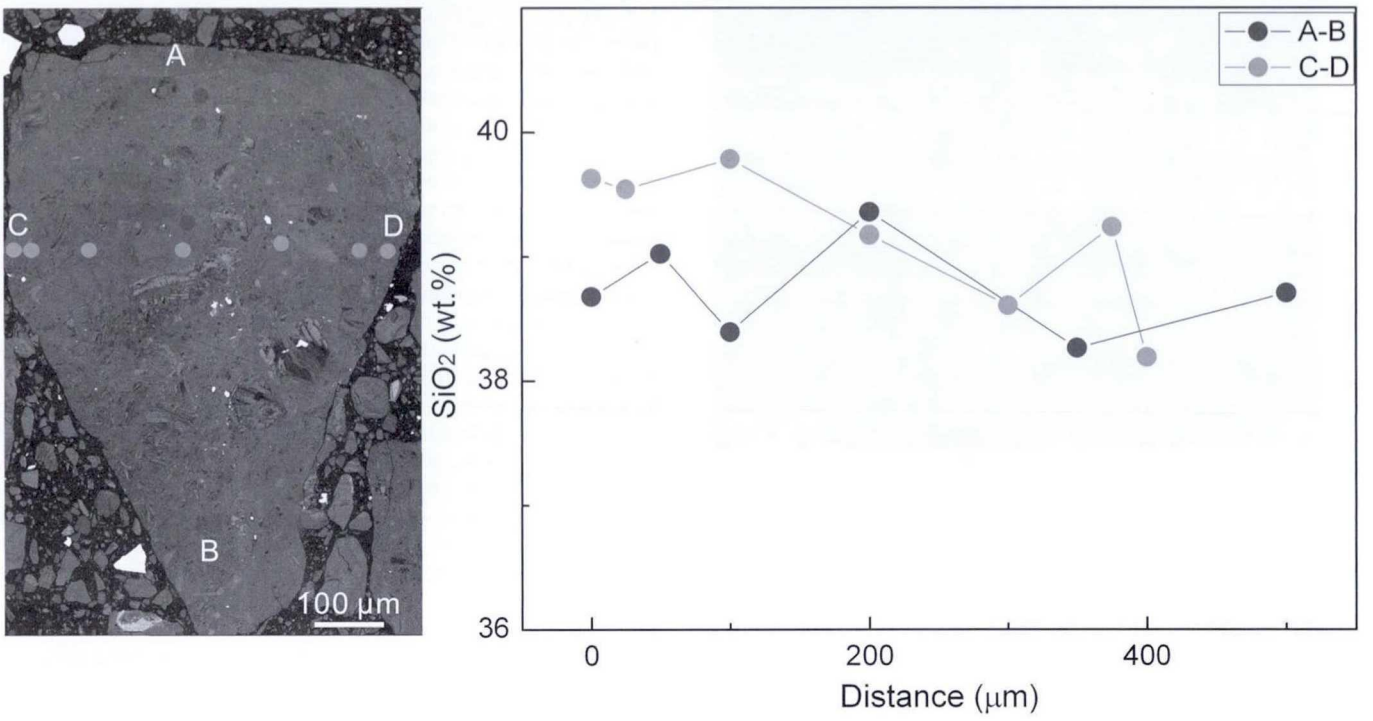

Figure 9. The distribution of SiO_2 along transects of completely serpentinized mineral fragments in the breccias, showing that SiO_2 is homogenously incorporated into serpentine minerals.

serpentinization. Pyroxene minerals obtained some iron from olivine during peridotite serpentinization, which may lead to a decrease in the production of iron oxide. The experimental results of this study agree well with previous work, which show that the production of iron oxide during the early stage of peridotite serpentinization is very low, and it increases greatly at the late stage of serpentinization (e.g., Toft et al., 1990; Oufi et al., 2002; Bach et al., 2006; Marcaillou et al., 2011; Ogasawara et al., 2013). It may result from the release of aluminum and silica during serpentinization. Chemical compositions of serpentine show that the Al_2O_3 contents of olivine-derived serpentine are positively correlated with the FeO contents. It suggests that the release of aluminum from pyroxene minerals increases the FeO contents of olivine-derived serpentine, which possibly decreases the production of iron oxide. By contrast, the correlation between the FeO and SiO_2 contents indicates that releases of SiO_2 from pyroxene minerals decrease the FeO contents of olivine-derived serpentine, which possibly increases the amounts of iron oxide produced. This study suggests that the production of iron oxide during peridotite serpentinization can be greatly influenced by fluxes of aluminum and silica. Aluminum may greatly control the production of iron oxide during the early stage of serpentinization, whereas silica is possibly more influential at the late stage of serpentinization.

Acknowledgements

This research was financially supported by the National Natural Science Foundation of China (Nos. 41603060, 91328204), Postdoctoral Science Foundation of China (Nos. 2015M570735, 2016T90805), the Strategic Priority Research Program of the Chinese Academy of Sciences (No. XDB06030100) and the scientific research fund of the Second Institute of Oceanography, SOA (JG1405). We thank S. Jiang from South China University of Technology for the help during FTIR analyses. We are appreciated for two anonymous reviewers for their constructive comments and suggestions.

References

Allen, D.E., Seyfried Jr., W.E., 2003. Compositional controls on vent fluids from ultramafic-hosted hydrothermal systems at mid-ocean ridges: an experimental study at 400 °C, 500 bars. Geochimica et Cosmochimica Acta 67, 1531–1542.

Anbalagan, G., Sivakumar, G., Prabakaran, A.R., Gunasekaran, S., 2010. Spectroscopic characterization of natural chrysotile. Vibrational Spectroscopy 52, 122–127.

Andreani, M., Daniel, I., Pollet-Villard, M., 2013. Aluminum speeds up the hydrothermal alteration of olivine. American Mineralogist 98, 1738–1744.

Bach, W., Paulick, H., Garrido, C.J., Ildefonse, B., Meurer, W.P., Humphris, S.E., 2006. Unraveling the sequence of serpentinization reactions: petrology, mineral chemistry, and petrophysics of serpentinites from MAR 15°N (ODP Leg 209, Site 1274). Geophysical Research Letters 33, L13306. http://dx.doi.org/10.1029/2006GL025681.

Beard, J.S., Frost, B.R., Fryer, P., McCaig, A., Searle, R., Ildefonse, B., Zinin, P., Sharma, S.K., 2009. Onset and progression of serpentinization and magnetite formation in olivine-rich troctolite from IODP Hole U1309D. Journal of Petrology 50, 387–403.

Berndt, M.E., Allen, D.E., Seyfried Jr., W.E., 1996. Reduction of CO_2 during serpentinization of olivine at 300 °C and 500 bar. Geology 24 (4), 351–354.

Bonifacie, M., Busigny, V., Mével, C., Philippot, P., Agrinier, P., Jendrzejewski, N., Scambelluri, M., Javoy, M., 2008. Chlorine isotopic composition in seafloor serpentinites and high-pressure metaperidotites. Insights into oceanic serpentinization and subduction processes. Geochimica et Cosmochimica Acta 72, 126–139.

Brazelton, W.J., Schrenk, M.O., Kelley, D.S., Baross, J.A., 2006. Methane- and sulfur-metabolizing microbial communities dominate the Lost City Hydrothermal Field ecosystem. Applied and Environmental Microbiology 72 (9), 6257–6270.

Brazelton, W.J., Nelson, B., Schrenk, M.O., 2010. Metagenomic evidence for H_2 oxidation and H_2 production by serpentinite-hosted subsurface microbial communities. Frontiers in Microbiology 2, 1–16.

Charlou, J.L., Donval, J.P., Fouquet, Y., Jean-Baptiste, P., Holm, N., 2002. Geochemistry of high H_2 and CH_4 vent fluids issuing from ultramafic rocks at the Rainbow hydrothermal field (36°14′N, MAR). Chemical Geology 191, 345–359.

Chen, D.G., Li, B.X., Zhi, X.C., 1994. Genetic geochemistry of mantle-derived peridotite xenolith from Panshishan, Jiangsu. Geochimica 23, 13–24.

Dungan, M.A., 1979. A microprobe study of antigorite and some serpentine pseudomorphs. Canadian Mineralogist 17, 771–784.

Escartín, J., Hirth, G., Evans, B., 1997. Effects of serpentinization on the lithosphere strength and the style of normal faulting at low-spreading ridges. Earth and Planetary Science Letters 151, 181–189.

Escartín, J., Hirth, G., Evans, B., 2001. Strength of slightly serpentinized peridotites: implications for the tectonics of oceanic lithosphere. Geology 29, 1023–1026.
Evans, B.W., 2008. Control of the products of serpentinization by the $Fe^{2+}Mg_{-1}$ exchange potential of olivine and orthopyroxene. Journal of Petrology 49, 1873–1887.
Evans, B.W., Kuehner, S.M., Chopelas, A., 2009. Magnetite-free, yellow lizardite serpentinization of olivine websterite, Canyon Mountain complex, N. E. Oregon. American Mineralogist 94, 1731–1734.
Evans, B.W., 2010. Lizardite versus antigorite serpentinites: magnetite, hydrogen, and life (?). Geology 38, 879–882.
Evans, B.W., Hattori, K., Baronnet, A., 2013. Serpentinite: what, why, where? Elements 9, 99–106.
Frost, B.R., Beard, J.S., 2007. On silica activity and serpentinization. Journal of Petrology 48, 1351–1368.
Frost, B.R., Evans, K.A., Swapp, S.M., Beard, J.S., Mothersole, F.E., 2013. The process of serpentinization in dunite from New Caledonia. Lithos 178, 24–39.
Fukuma, K., Dunlop, D.J., 2006. Three-dimensional micromagnetic modeling of randomly oriented magnetite grains (0.03–0.3 μm). Journal of Geophysical Research 111, B12S11. http://dx.doi.org/10.1029/2006JB004562.
Ge, K.P., Liu, Q.S., 2014. Effects of the grain size distribution on magnetic properties of magnetite: constraints from micromagnetic modeling. Chinese Science Bulletin 59 (34), 4763–4773.
Germanovich, L.N., Genc, G., Lowell, R.P., Rona, P.A., 2012. Deformation and surface uplift associated with serpentinization at mid-ocean ridges and subduction zones. Journal of Geophysical Research 117, B07103. http://dx.doi.org/10.1029/2012JB009372.
Guillot, S., Hattori, K., 2013. Serpentinites: essential roles in geodynamics, arc volcanism, sustainable development, and the origin of life. Elements 9, 95–98.
Hattori, K.H., Guillot, S., 2003. Volcanic fronts as a consequence of serpentinites dehydration in the fore-arc mantle wedge. Geology 31, 525–528.
Hébert, R., Adamson, A.C., Komor, S.C., 1990. Metamorphic petrology of ODP Leg 109, Hole 670A serpentinized peridotites: serpentinization processes at a slow spreading ridge environment. Proceedings of the Ocean Drilling Program, Scientific Results 106/109, 103–115.
Holm, N.G., Oze, C., Mousis, O., Waite, J.H., Guilbert-Lepoutre, A., 2015. Serpentinization and the formation of H_2 and CH_4 on celestial bodies (planets, moons, comets). Astrobiology 15, 587–600.
Huang, R.F., Sun, W.D., Ding, X., Wang, Y.R., Zhan, W.H., 2015a. Experimental investigation of iron mobility during serpentinization. Acta Petrologica Sinica 31 (3), 883–890.
Huang, R.F., Sun, W.D., Ding, X., Liu, J.Z., Peng, S.B., 2015b. Olivine versus peridotite during serpentinization: gas formation. Science China: Earth Sciences 58, 2165–2174.
Hyndman, R.D., Peacock, S.M., 2003. Serpentinization of the forearc mantle. Earth and Planetary Science Letters 212, 417–432.
Klein, F., Bach, W., Jöns, N., McCollom, T., Moskowitz, B., Berquó, T., 2009. Iron partitioning and hydrogen generation during serpentinization of abyssal peridotites from 15°N on the Mid-Atlantic Ridge. Geochimica et Cosmochimica Acta 73, 6868–6893.
Klein, F., Bach, W., Humphris, S.E., Kahl, W.A., Jöns, N., Moskowitz, B., Berquó, T.S., 2014. Magnetite in seafloor serpentinite—some like it hot. Geology 42, 135–138.
Lafay, R., Montes-Hernandez, G., Janots, E., Chiriac, R., Findling, N., Toche, F., 2012. Mineral replacement rate of olivine by chrysotile and brucite under high alkaline conditions. Journal of Crystal Growth 347, 62–72.
Lafay, R., Montes-Hernandez, G., Janots, E., Chiriac, R., Findling, N., Toche, F., 2014. Simultaneous precipitation of magnesite and lizardite from hydrothermal alteration of olivine under high-carbonate alkalinity. Chemical Geology 368, 63–75.
Malvoisin, B., Brunet, F., Carlut, J., Rouméjon, S., Cannat, M., 2012. Serpentinization of oceanic peridotites: 2. Kinetics and progresses of San Carlos olivine hydrothermal alteration. Journal of Geophysical Research 117, B04102. http://dx.doi.org/10.1029/2011JB008842.
Malvoisin, B., 2015. Mass transfer in the oceanic lithosphere: serpentinization is not isochemical. Earth and Planetary Science Letters 430, 75–85.
Marcaillou, C., Muñoz, M., Vidal, O., Parra, T., Harfouche, M., 2011. Mineralogical evidence for H_2 degassing during serpentinization at 300 °C/300 bar. Earth and Planetary Science Letters 303, 281–290.
McCollom, T.M., Bach, W., 2009. Thermodynamic constraints on hydrogen generation during serpentinization of ultramafic rocks. Geochimica et Cosmochimica Acta 73, 856–875.
McCollom, T.M., Klein, F., Robbins, M., Moskowitz, B., Berquó, T.S., Jöns, N., Bach, W., Templeton, A., 2016. Temperature trends for reaction rates, hydrogen generation, and partitioning of iron during experimental serpentinization of olivine. Geochimica et Cosmochimica Acta 181, 175–200.
Mével, C., 2003. Serpentinization of abyssal peridotites at mid-ocean ridges. Comptes Rendus Geoscience 335, 825–852.
Miyoshi, A., Kogiso, T., Ishikawa, N., Mibe, K., 2014. Role of silica for the progress of serpentinization reactions: constraints from successive changes in mineralogical textures of serpentinites from Iwanaidake ultramafic body, Japan. American Mineralogist 99, 1035–1044.
Müntener, O., 2010. Serpentine and serpentinization: a link between planet formation and life. Geology 38, 959–960.
Okamoto, A., Ogasawara, Y., Ogawa, Y., Tsuchiya, N., 2011. Progress of hydration reactions in olivine-H_2O and orthopyroxenite-H_2O systems at 250 °C and vapor-saturated pressure. Chemical Geology 289, 245–255.
Ogasawara, Y., Okamoto, A., Hirano, N., Tsuchiya, N., 2013. Coupled reactions and silica diffusion during serpentinization. Geochimica et Cosmochimica Acta 119, 212–230.
Oufi, O., Cannat, M., Horen, H., 2002. Magnetic properties of variably serpentinized abyssal peridotites. Journal of Geophysical Research: Solid Earth 107 (B5), 2095. http://dx.doi.org/10.1029/2001JB000549.
Rouméjon, S., Cannat, M., Agrinier, P., Godard, M., Andreani, M., 2015. Serpentinization and fluid pathways in tectonically exhumed peridotites from the Southwest Indian Ridge (62–65° E). Journal of Petrology 56, 703–734.
Scambelluri, M., Fiebig, J., Malaspina, N., Müntener, O., Pettke, T., 2004. Serpentinite subduction: implications for fluid processes and trace-element recycling. International Geology Review 46, 595–613.
Schmidt, M.W., Poli, S., 1998. Experimentally based water budgets for hydrating slabs and consequences for arc magma generation. Earth and Planetary Science Letters 163, 361–379.
Schrenk, M.O., Kelley, D.S., Bolton, S.A., Baross, J.A., 2004. Low archaeal diversity linked to subseafloor geochemical processes at the Lost City hydrothermal field, Mid-Atlantic Ridge. Environmental Microbiology 6 (10), 1086–1095.
Schrenk, M.O., Brazelton, W.J., Lang, S.Q., 2013. Serpentinization, carbon, and deep life. Reviews in Mineralogy & Geochemistry 75, 575–606.
Seyfried Jr., W.E., Dibble Jr., W.E., 1980. Seawater-peridotite interaction at 300 °C and 500 bars: implications for the origin of oceanic serpentinites. Geochimica et Cosmochimica Acta 44, 309–321.
Seyfried Jr., W.E., Foustoukos, D.I., Fu, Q., 2007. Redox evolution and mass transfer during serpentinization: an experimental and theoretical study at 200 °C, 500 bar with implications for ultramafic-hosted hydrothermal systems at mid-ocean ridges. Geochimica et Cosmochimica Acta 71, 3872–3886.
Seyfried Jr., W.E., Pester, N.J., Ding, K., Rough, M., 2011. Vent fluid chemistry of the Rainbow hydrothermal system (36°N, MAR): phase equilibria and in situ pH controls on subseafloor alteration processes. Geochimica et Cosmochimica Acta 75, 1574–1593.
Sun, W.D., Peng, Z.C., Zhi, X.C., Chen, D.G., Wang, Z.R., Zhou, X.H., 1998. Osmium isotope determination on mantle-derived peridotite xenoliths from Panshishan with N-TIMS. Chinese Science Bulletin 43, 573–575.
Toft, P.B., Arkani-Hamed, J., Haggerty, S.E., 1990. The effects of serpentinization on density and magnetic susceptibility: a petrophysical model. Physics of the Earth and Planetary Interiors 65 (1–2), 137–157.
Ulmer, P., Trommsdorff, V., 1995. Serpentine stability to mantle depths and subduction-related magmatism. Science 268, 858–861.
Xu, X.S., Griffin, W.L., O'Reilly, S.Y., Pearson, N.J., Geng, H.Y., Zheng, J.P., 2008. Re-Os isotopes of sulfides in mantle xenoliths from eastern China: progressive modification of lithospheric mantle. Lithos 102, 43–64.
Yang, X.Y., 2008. Geochemical Study on Cenozoic Mantle Derived Peridotitic Xenoliths from Panshishan and Lianshan, Jiangsu Province. M.S. thesis. Guangzhou Institute of Geochemistry, Chinese Academy of Sciences.